Harmonic growth of ion-cyclotron waves in Saturn's magnetosphere

Mario Rodríguez-Martínez,[1] X. Blanco-Cano,[1] C. T. Russell,[2] J. S. Leisner,[3] R. J. Wilson,[4] and M. K. Dougherty[5]

Received 19 October 2009; revised 5 February 2010; accepted 30 March 2010; published 9 September 2010.

[1] Ion-cyclotron waves have been observed by the Cassini spacecraft in Saturn's middle magnetosphere. Waves have frequencies near the gyrofrequencies of water-group ions, they are left handed, and in most regions they propagate at small angles to the ambient magnetic field. Their origin is explained in terms of the ion-cyclotron instability generated by water-group ions picked up from Saturn's neutral cloud. Additionally, in some regions dynamic spectra reveal the existence of fluctuations at approximately twice the value of the ion gyrofrequency. These waves have a significant compressional component and propagate at oblique angles to the magnetic field. Their characteristics suggest that these fluctuations can be identified as a harmonic mode ($n = 2$) generated by the ring distributions of pickup ions. In this work we study in detail the characteristics of these harmonic mode waves. We also evaluate growth rates using a kinetic dispersion analysis.

Citation: Rodríguez-Martínez, M., X. Blanco-Cano, C. T. Russell, J. S. Leisner, R. J. Wilson, and M. K. Dougherty (2010), Harmonic growth of ion-cyclotron waves in Saturn's magnetosphere, *J. Geophys. Res.*, *115*, A09207, doi:10.1029/2009JA015000.

1. Introduction

[2] The Cassini mission has allowed the study of plasma instabilities in the rapidly rotating magnetosphere of Saturn. From magnetic field observations [*Dougherty et al.*, 2004], recent studies have shown that the middle magnetosphere is rich in wave phenomena with ion-cyclotron waves (ICW) and mirror mode waves appearing at different radial distances from Saturn [*Russell et al.*, 2006; *Leisner et al.*, 2006]. The ion-cyclotron instability in these regions is generated by water-group ions (O^+, OH^+, H_2O^+, or H_3O^+) picked up from the E-ring neutral cloud that form rings in velocity space. Ion-cyclotron waves are important as diagnostic of processes operating in the magnetosphere and can provide insight of the composition of the plasma producing the waves [*Russell and Blanco-Cano*, 2007].

[3] From the orbital insertion of Cassini spacecraft around Saturn on 1 July 2004, at least three flybys of the Enceladus moon during 2005 and others inside Saturn's middle magnetosphere have shown that Enceladus is the source of material for the E ring with a plume ejecta (near the south pole) that affects the properties of local magnetospheric plasma, such as mass density and flow patterns [*Khurana et al.*, 2007; *Kivelson*, 2006]. The rate of water loss from Enceladus in the plume has been estimated by *Hansen et al.* [2006] as a function of the plume area and the thermal velocity between 150 and 350 kg/s (approximately 5×10^{27} and 1×10^{28} particles/s, respectively). However, other calculations using the observed wave amplitudes made by *Leisner et al.* [2006] reveal that the E-ring neutral cloud losses 2.26×10^{26} particles/s. This is an underestimate value due to the limited radial range of wave observations and the model. Nevertheless, this rate is about two orders of magnitude less than the mass production in the Io torus. In addition, a total mass loading rate of about 100 kg s^{-1} (3×10^{27} H_2O molecules per second) was inferred by *Tokar et al.* [2006].

[4] Jupiter's Io moon is another example where ion-cyclotron waves are generated by mass–loading. In this case waves are seen at the gyrofrequency of SO_2^+, SO^+, and S^+ ions with amplitudes approaching 100 nT peak to peak. The waves begin about 20 Io radii outward from Io [*Huddleston et al.*, 1999; *Russell and Blanco-Cano*, 2007]. Observations during the Galileo J0 pass found waves with propagation angles of $\theta = 0°$–$20°$ and ellipticity between −0.6 and −0.8. While most of the ion-cyclotron waves propagated typically at these angles, there were intervals when waves propagated at angles up to 40° to the ambient magnetic field $\mathbf{B}_\circ$ [*Blanco-Cano et al.*, 2001a, 2001b]. Hybrid simulations by *Cowee et al.* [2007] have predicted the existence of the first SO^+ harmonic near Io. However, no harmonic mode waves have been reported from observations.

[1]Instituto de Geofísica, Departamento de Ciencias Espaciales, Universidad Nacional Autónoma de México, Coyoacán, México.
[2]Institute of Geophysics and Planetary Physics, University of California, Los Angeles, California, USA.
[3]Department of Physics and Astronomy, University of Iowa, Iowa City, Iowa, USA.
[4]Laboratory for Atmospheric and Space Physics, University of Colorado at Boulder, Boulder, Colorado, USA.
[5]Blackett Laboratory, Department of Physics, Imperial College, London, UK.

0148-0227/10/2009JA015000

Table 1. Summary of Observations Where ICW Are Observed at the Fundamental and Their First HMW

Date	ICW[a]	(ICW+HMW)[b]	Distance[c] (R_S)	Latitude[d] (°)	Distance[e] (km)	B_o[f] (nT)
09-Mar-05	06:00 to 07:30	07:30 to 09:00	4.60–4.01	−0.151 to −0.100	500	449.91
	14:30 to 15:00	15:00 to 16:00	4.26–4.68	0.194 to 0.206	—	—
17-Feb-05	04:10 to 06:00	03:00 to 04:10	3.82–4.20	0.248 to 0.329	1179	473.94
24-Dec-05	16:40 to 19:00	19:00 to 24:00	4.82–4.87	−0.024 to 0.313	97200	181.87
27-Nov-05	14:30 to 16:30	09:00 to 14:30	4.82–5.00	−0.021 to 0.333	108600	184.20

[a]Time interval of ICW at the fundamental for all observations.
[b]Time interval where ICW plus harmonics modes were observed.
[c]Radial distances between Cassini and Saturn corresponding to the intervals where there are ICW+HMW (1 R_S = 60268 km).
[d]Geographic latitude for Cassini's position for the intervals of ICW+HMW.
[e]Minimun distance between Cassini and Enceladus for each flyby.
[f]Value of the magnetic field magnitude when Cassini is crossing the equator of Saturn.

[5] On the other hand, the occurrence of ion-cyclotron waves with harmonic modes has been observed in planetary foreshocks and cometary environments. The first evidence of harmonic modes in planetary environments was reported by *Smith et al.* [1983], who found low-frequency waves on Voyager measurements upstream of the Jovian bow shock. These modes were explained in terms of oblique harmonic cyclotron resonance with a proton ring beam. Cyclotron harmonic waves were also reported from Giotto measurements upstream of the quasi-parallel bow shock region of comet P/Halley [*Wong et al.*, 1991; *Glassmeier et al.*, 1989]. In this case the waves were associated with heavy (water group) newborn ions. In addition, *Tan et al.* [1993] identified cyclotron wave harmonics due to pickup ions (H^+, H_2^+, and O^+) near comet Giacobini-Zinner using ICE spacecraft. These harmonics of cyclotron waves are consistent with the multiples of 6, 7, 8, 9, 10, and 12 of ion gyrofrequencies of O^+ and multiples of 1, 1.5, 2, and 2.5 of the proton gyrofrequencies and they have been analyzed in *Brinca* [1991] and *Tsurutani* [1991].

[6] Studying ion-cyclotron waves at Saturn's magnetosphere can help to gain insight about how these waves (at the fundamental gyrofrequencies and as harmonics) can grow in other mass loading environments such as comets, where water-group ions can generate similar fluctuations and where observations are sparse. At Saturn's magnetosphere the corrotation velocity is perpendicular to the magnetic field so that ions are picked up into ring distributions able to generate waves. In contrast, at comets the situation is more complex; ions can be injected at different angles depending on the orientation of the flow velocity and the magnetic field, and in some cases pickup ions can have a significant parallel drift velocity, so more wave modes are unstable [*Huddleston and Johnstone*, 1992]. Thus, results obtained by studying ion-cyclotron waves in planetary magnetospheres can be valuable to understand wave generation and evolution near comets when the solar wind velocity and the interplanetary magnetic field are perpendicular.

[7] In this work we show that ion-cyclotron harmonic mode waves, with frequencies at twice the value of the water-group ion gyrofrequency, $f \sim 2 \times \Omega_{W^+}$, also exist in the Kronian magnetosphere in addition to the reported ion-cyclotron waves with frequencies close to the fundamental gyrofrequency of water-group ions, $f \sim \Omega_{W^+}$ [*Russell et al.*, 2006; *Leisner et al.*, 2006]. In section 2 we describe the properties of harmonic mode waves and compare wave characteristics with fluctuations observed at the fundamental gyrofrequency. In section 3 we use kinetic dispersion analysis to gain insight about wave growth. Finally our results are discussed and summarized in section 4.

2. Observations of Harmonic Mode Waves

2.1. Overview

[8] We use magnetic field measurements, taken during 2005, from the Dual Technique Magnetometer (MAG) onboard the Cassini spacecraft at a resolution of 1 vector per second [*Dougherty et al.*, 2004]. Two of these flybys were very close to Enceladus, those on 17 February (E0) and 9 March (E1) (see Table 1). The other two observations occurred on 24 December and 27 November. Additionally, we use the Cassini Plasma Spectrometer (CAPS) [*Young et al.*, 2004; *Wilson et al.*, 2008] data for the last two observations. During these four orbits we find extended regions where ion-cyclotron waves with frequencies at approximately twice the value of water-group ions are observed ($2 \times \Omega_{W^+}$). We interpret these waves as harmonic ion-cyclotron mode. We use W^+ (water-group ions) to identify a combination of O^+, OH^+, H_2O^+, and H_3O^+ ions.

[9] Figure 1 shows dynamic spectra (DS) of 5 h of observations during these 4 days. The top (bottom) plot for each day corresponds to the transverse (compressional) power spectral density. Horizontal white lines on Figure 1 indicate the gyrofrequencies of ions O^+, H_3O^+, and O_2^+ (Ω_{16^+}, Ω_{19^+}, and Ω_{32^+} respectively). Ion-cyclotron waves at the fundamental frequency of O^+, H_3O^+, and O_2^+ appear during ~7 h for 24 December and 27 November observations, but details for only 5 h are shown for those dates. In contrast, the observation of 9 March shows ion-cyclotron waves at the fundamental for a short interval of 3 h with a cutoff of ~2 h between 09:30 UT and 11:30 UT corresponding to a distance of 3.8 R_S from Saturn's center consistent with the distances reported by *Russell and Blanco-Cano* [2007]. Finally the observation of 17 February shows the existence of ion-cyclotron waves at the fundamental mode of O^+, H_3O^+, and O_2^+ ions in a similar range to the March observation but with a cutoff of ~1.5 h between 00:30 UT and 02:00 UT for O^+ and H_3O^+. Previous work on ion-cyclotron waves at the Saturnian magnetosphere interpreted the waves in terms of H_2O^+ ions. However, waves frequency on the spectra on Figure 1 match better the gyrofrequency of H_3O^+ ions (see also Figure 4). This is in agreement with the *Fleshman et al.* [2010] work which reports that H_3O^+ is the dominant water species ion downstream of the Enceladus plume. During this interval the transverse power spectral peaks at frequencies near the gyrofrequency of O_2^+ ions ($f \sim \Omega_{32^+}$), indicating that the com-

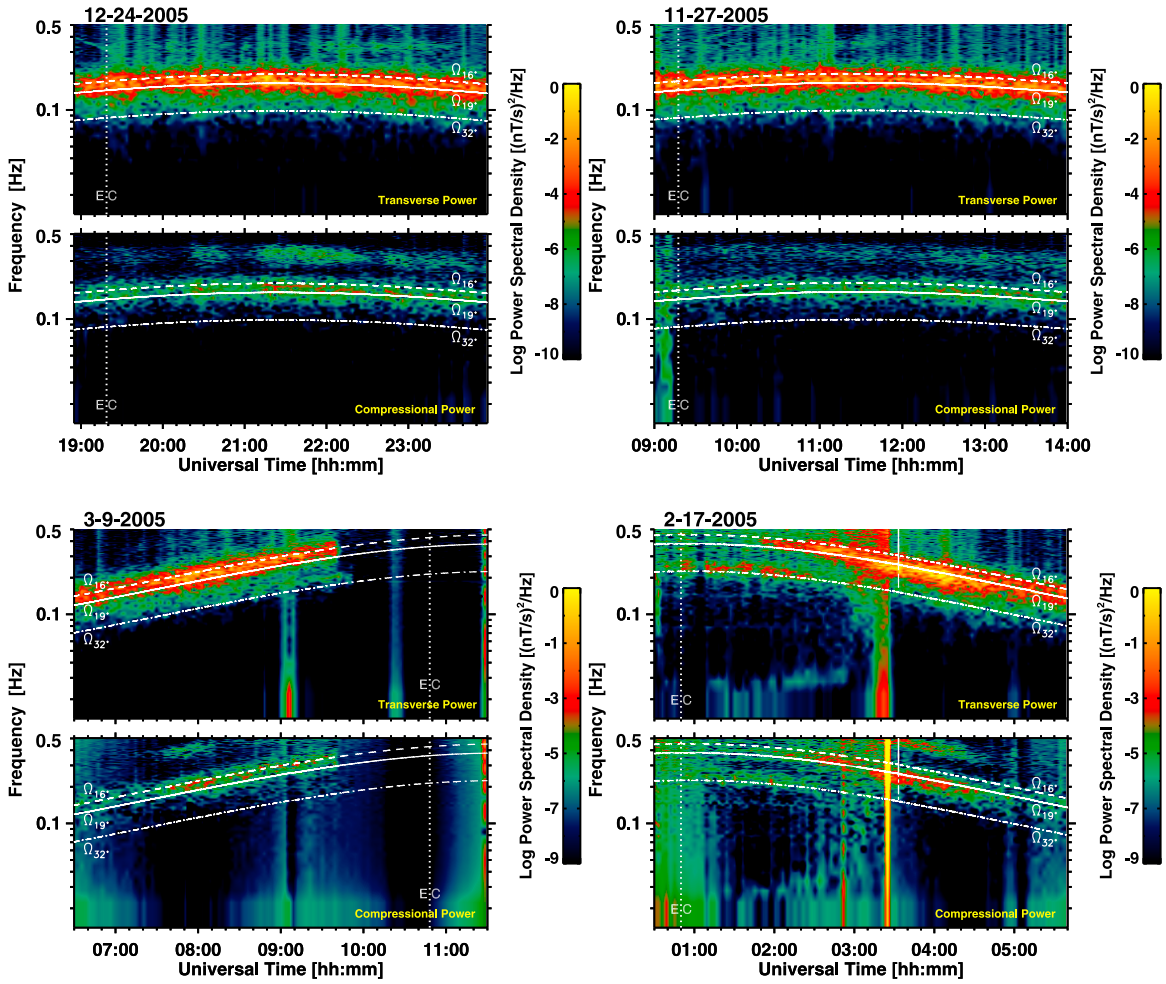

Figure 1. Dynamic spectra for 5 h of Cassini observations on 24 December 2005, 27 November 2005, 9 March 2005, and 17 February 2005 where harmonics can be seen in the compressive power. For each day we show both transverse and compressive power. The observations are consistent with ion-cyclotron waves observed at the gyrofrequencies of Ω_{16^+}, Ω_{19^+}, and Ω_{32^+} ions (white lines). Cassini travels toward the right and the line E C represents the equator crossing by Cassini.

position of the ring distribution generating the waves can vary.

[10] Harmonic mode waves (HMW) at $2 \times \Omega_{W^+}$ appear over different lengths of time intervals. The observations of 17 February and 9 March on Figure 1, where Cassini traveled toward the right, show waves with $f \sim 2 \times \Omega_{19^+}$ in short intervals of ~1 h corresponding to 03:20–04:20 h and 07:30–08:30 h, respectively, and radial distances between 3.8 R_S and 4.6 R_S from Saturn (1 R_S = 60,268 km). The 24 December and 27 November observations have larger intervals of harmonics lasting ~5 h, between 19:00–24:00 h and 09:00–14:00 h, respectively, corresponding to distances from Saturn slightly larger, between 4.8 R_S and 5.5 R_S. In addition, during the 9 March flyby, harmonic mode waves were also observed during 15:00–16:00 h, i.e., at distances ~3.8 R_S–4.6 R_S (see Table 1). Power spectra show that the ion-cyclotron waves at the fundamental are mainly transverse fluctuations, while the harmonic mode waves have a larger compressive power. Table 1 summarizes the time intervals and distances for ICW plus their first HMW. We observe that the magnetic field magnitude, $\mathbf{B}_\circ$, had different values for each region of the observations. For the ICW region, $\mathbf{B}_\circ$ was between 109.33 and 299.10 nT while for the ICW+HMW region, the field is stronger with values between 157.19 and 363.60 nT.

[11] Figure 2 shows the orbits for each observation on the *XY* plane. For these plots we use the Kronian solar rotational (KSR) system, where *Z* is along Saturn's rotation axis; *X* is perpendicular to *Z* in the plane containing *Z* and the Sun-Saturn line and is positive toward the Sun; and *Y* completes the right-hand system and is positive duskward. The positions of Enceladus, when Cassini begins and ends the detection of ICW+HMW, are marked with open and filled circles, respectively. The regions with ICW and ICW+HMW are indicated along the Cassini's orbit to show where we applied DS, fast Fourier transform (FFT) and minimum variance (MVA) analysis to characterize the ion-cyclotron waves and their harmonic mode. For these four observations Cassini was at a radial distance from Saturn between 3.8 R_S and 5.5 R_S when the harmonic mode waves appear at the DS. We found that for each orbit the ICW+HMW region occurs closer to Enceladus than ICW. For example, for the observation of 9 March, ICM+HMW occur at ~13 R_E, while ICW occur at

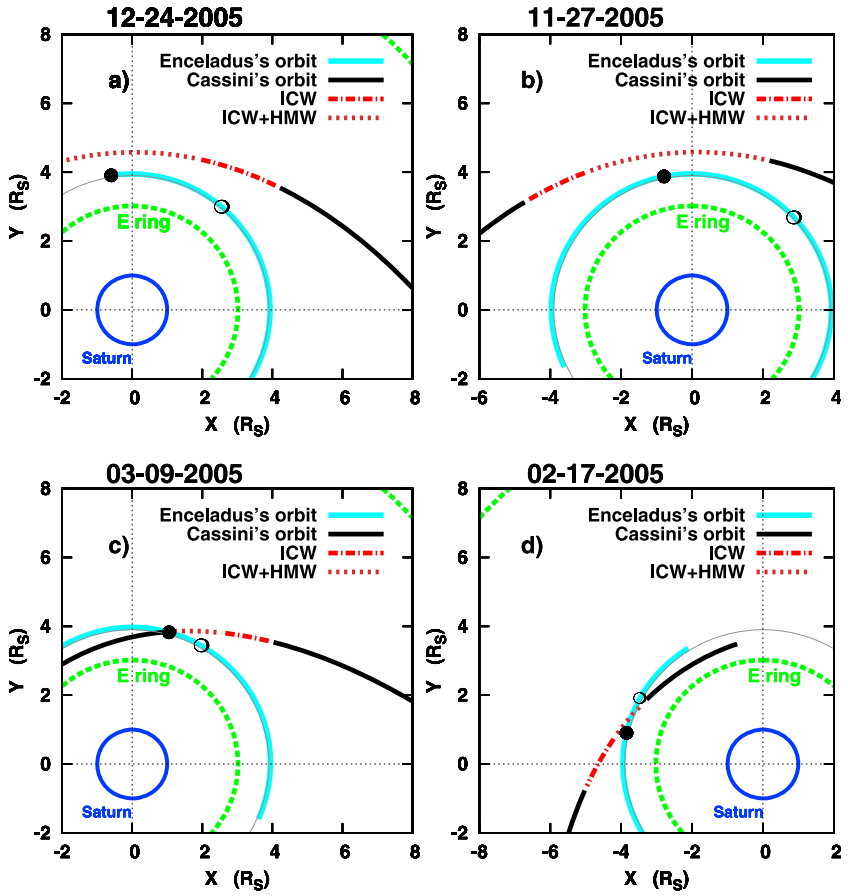

Figure 2. Orbits of Cassini and Enceladus in the *XY* plane. (a) 24 December 2005; (b) 27 November 2005; (c) 9 March 2005; and (d) 17 February 2005. The open and filled circles in each plot indicate the positions of Enceladus when Cassini begins and ends, respectively, the detection of ICW+HMW in its orbit. In each plot, both Cassini and Enceladus travel counterclockwise.

distances ~157 R_E (1 R_E = 251.8 km, the Enceladus radii). In all cases the inclination of Cassini's orbit at the moment of equator crossing (E C) position is small (<0.5°), so Cassini crossed almost parallel to the E ring. During these four orbits, the regions of ICW and their first HMW were observed very close to the geographic equator (±0.04 R_S). Previous work (J. S. Leisner, personal communication, 2009) has shown that ICW can be observed up to ±0.20 R_S from the equator plane. More work is needed to determine if HMW can occur up to ±0.20 R_S from the magnetic equator for orbits with low and high angles of inclination.

2.2. Wave Properties

[12] Figure 3 shows magnetic field time series for 5 min intervals where ICW+HMW were observed. From top to bottom, each grid shows B_x, B_y, B_z, and **B** with a quadratic fit removed. This region exhibits wave amplitudes up to ~0.7 nT which are slightly larger than those reported previously [*Dougherty et al.*, 2006; *Leisner et al.*, 2006] of ~0.5 nT, for the E0, E1, and 24 December flybys where they found ICW just at the fundamental gyrofrequency. A distinctive characteristic of these waves is the quasi-periodic variation in amplitude that must originate from wave beating on two or more waves with different frequencies interact with comparable speeds.

[13] The FFT analysis is given in transverse and compressive powers for a better contrast and characterization of the waves. The compressive power is defined from the total power, P_{tot}, which is the result of applying FFT to the total magnetic field $\mathbf{B}_\circ$, while the transverse power is defined as $|P_x + P_y + P_z - P_{\mathrm{tot}}|$, where P_x, P_y, and P_z, are the powers of B_x, B_y, and B_z. Figure 4 displays FFT analysis for the intervals on Figure 3. The transverse and compressive powers show a main peak consistent with the gyrofrequencies of O_2^+ ions, Ω_{32^+}, and water-group ions, such as Ω_{16^+} and Ω_{19^+}. It is possible to see that in all cases ICW with frequencies close to the fundamental gyrofrequency are mainly transverse with the transverse power at least one order of magnitude larger than its compressive counterpart. The observed profile for the fundamental peak in all cases is wide, and a double peak in the transverse power is found for 17 February and 27 November, where this secondary peak corresponds to the gyrofrequency of O_2^+ ions (Ω_{32^+}). This indicates that O_2^+ ions are commonly picked up in the regions of analysis which is consistent with the fact that O_2 is an important component at lower altitudes as stated by *Martens et al.* [2008], *Johnson et al.* [2006], and *Young et al.* [2005]. In addition, Figure 4 also shows a secondary peak in the compressive power which appears at twice the gyrofrequency of H_3O^+ ions ($2 \times \Omega_{19^+}$), suggesting the existence of ICW growing at a harmonic $f \sim n \times \Omega_{W^+}$, with

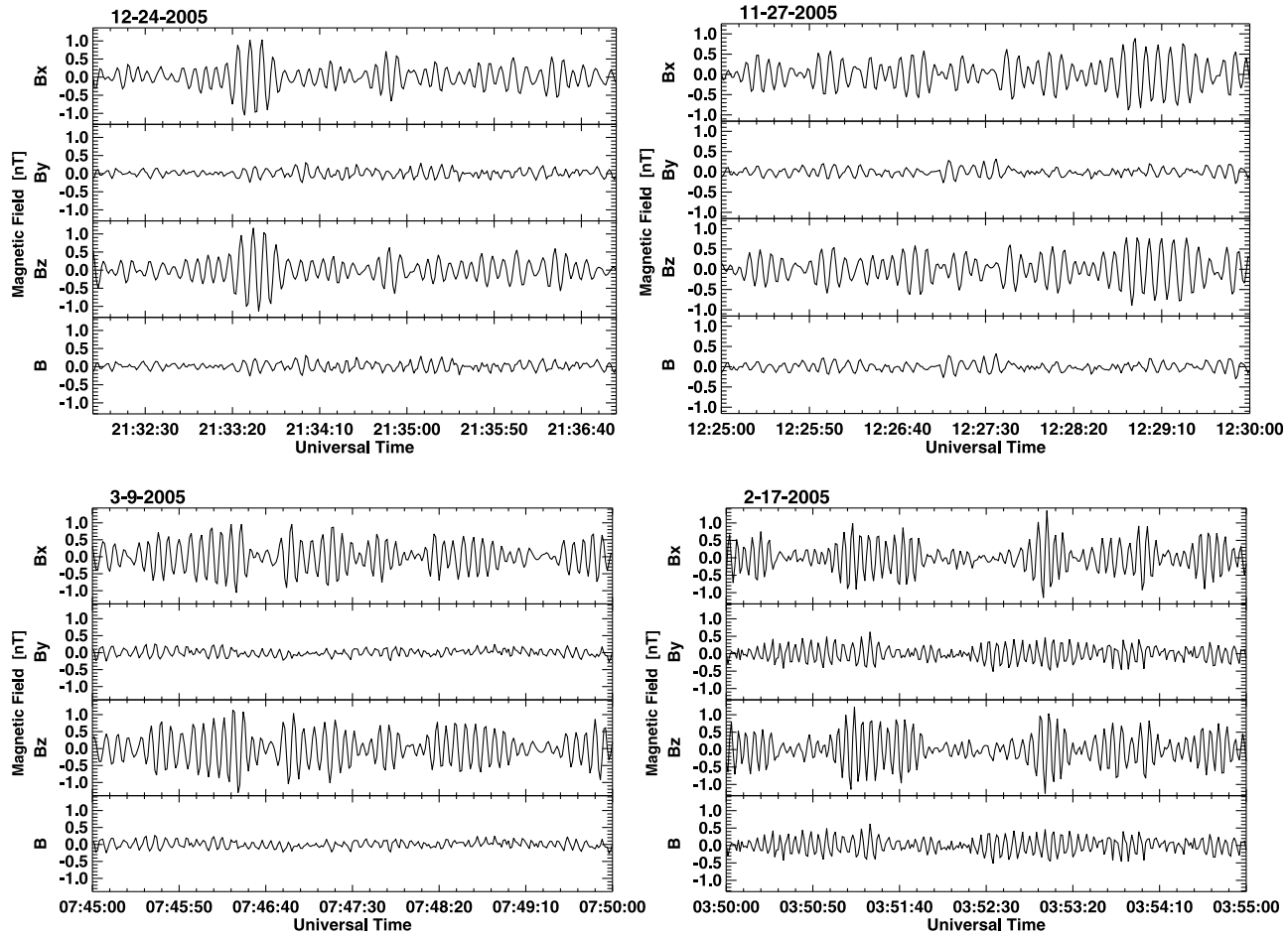

Figure 3. Magnetic field components and magnitude for representative 5 min intervals, where ion-cyclotron waves at the fundamental and $n = 2$ harmonics were observed. Here we plotted the perturbation in the magnetic field, and the background field is removed using a quadratic fit.

$n = 2$. For this peak the compressive power is larger than in the transverse component, almost by one order of magnitude in all cases except for the 27 November observation, where the difference between compressive and transverse powers is smaller. For all days except 17 February, the peaks at $2 \times \Omega_{19^+}$ are wide-reaching frequencies close to $2 \times \Omega_{16^+}$ or $2 \times \Omega_{18^+}$. What is more, the double peak present in the compressive power suggests that waves are being generated at more than one of these frequencies ($2 \times \Omega_{16^+}$, $2 \times \Omega_{18^+}$, $2 \times \Omega_{19^+}$).

[14] On the other hand, on 17 February there are time intervals where DS show that O_2^+ waves can have larger amplitudes than waves with $f \sim \Omega_{19^+}$. Figure 5 presents one of these intervals where the main peak is wide for both transverse and compressional powers and occurs at the gyrofrequency of O_2^+ ions (Ω_{32^+}) at radial distances of 3.5–3.6 R_S, and close to the geographic equator (0–0.0104 R_S). The fact that O_2^+ waves can be dominant in some intervals reveals that the composition of the rings producing the waves is variable and that some times O_2^+ dense rings can form overcoming the instability threshold while instability due to H_3O^+ ions is stable.

[15] In order to know wave propagation angles and polarization properties we use minimum variance analysis (MVA) [*Hoppe et al.*, 1981]. Figure 6 shows hodograms in the principal axes coordinates for two regions with ion-cyclotron waves at the fundamental plus harmonic mode waves (ICW +HMW). Figure 7 shows two intervals where only ICW at the fundamental were observed. In all cases waves are left handed. The waves in regions with ICW+HMW are compressive, elliptically polarized with angles of propagation with respect to the ambient field, between 17° and 59°. For the cases shown on Figure 6 the angles of propagation were 34.7° and 27.8°. In contrast, the waves in regions with only ICW are more transverse and circularly polarized and propagate closer to the ambient field direction, with $\theta_{B_{oK}} < 13°$. For the two intervals of Figure 7 the ICW propagate at $\theta_{B_{oK}} = 10°$ and 6°. The compressive nature of regions with HMW is consistent with the FFT and DS analysis, where the compressive power is always larger for the peak at $2 \times \Omega_{W^+}$.

[16] Table 2 shows a summary of MVA analysis for 30 s within the intervals of Figure 3 for the harmonic mode region and for the fundamental ICW region. Waves at the fundamental are more planar so the propagation angle is well determined. In contrast, the fluctuations in the regions with IC+HM waves show a large variance reflecting the fact that the magnetic profiles observed by the spacecraft are composed by waves with different characteristics arriving from different locations (i.e., mainly parallel propagating waves generated at the fundamental gyrofrequency by ion resonance plus harmonic mode waves that propagate obliquely to the

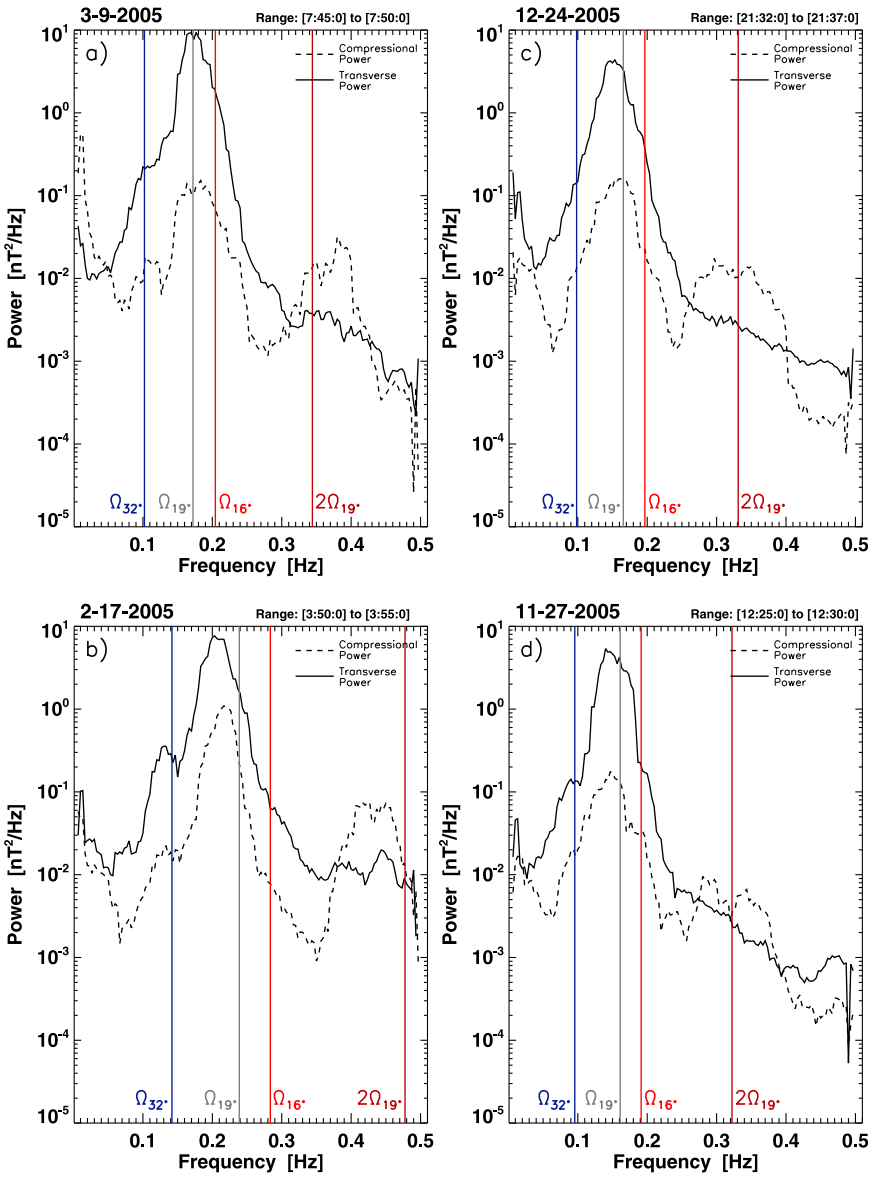

Figure 4. Power spectral density for (a) 9 March 2005 on the range of [07:45–07:55] h, (b) 17 February 2005 [03:45–03:50] h, (c) 24 December 2005 [21:32–21:37] h and (d) 27 November 2005 [12:25–12:30] h. The gyrofrequencies of Ω_{16^+}, Ω_{19^+}, Ω_{32^+}, and $2 \times \Omega_{19^+}$ are indicated with dashed lines (for a complete explanation about the peaks see the text).

field). In other words, the observed waves may be described by a wave distribution formed by waves propagating at different angles and spread in frequency (see, for example, the work of *Storey and Lefeuvre* [1979]).

3. Kinetic Dispersion Theory

[17] The ion-cyclotron waves at Saturn's middle magnetosphere grow from temperature anisotropies ($T_\perp/T_\parallel \gg 1$) produced by ion rings picked up from the neutral cloud. The existence of these waves is important as a diagnostic of the mass-loading process that occurs in giant magnetospheres due to the presence of satellites with atmospheres and ring material [*Leisner et al.*, 2006; *Blanco-Cano*, 2004]. In order to characterize the properties of plasma instabilities and conditions for wave growth, it is necessary to use kinetic dispersion theory [*Gary*, 1993; *Brinca and Tsurutani*, 1989a, 1989b].

[18] Plasma conditions in space environments are commonly suitable for the development of waves and instabilities. Regions like the E ring of Saturn where mass loading occurs are very favorable for wave growth. To estimate the necessary conditions for the growth of ion-cyclotron waves at both the fundamental ($n = 1$) and the first harmonic ($n = 2$), we have used the dispersion solver WHAMP [*Rönmark*, 1982]. We consider a six-species plasma resembling the E-ring region (see Table 3), with a H_3O^+ cold ring distribution. WHAMP models bi-Maxwellian velocity distributions rather than ring beams, but as shown by *Cowee et al.* [2007], this dispersion code provides results that are similar to those obtained when newborn ions are modeled as a ring if one considers a highly anisotropic bi-Maxwellian equivalent to a ring with $T_\perp =$

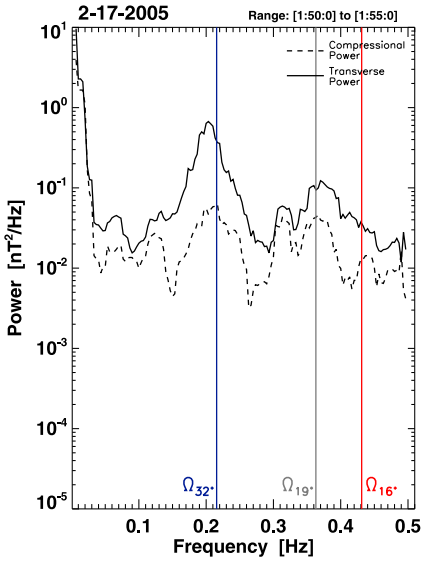

Figure 5. Power spectral density for 17 February 2005 on the range of [01:50–01:55] h. The gyrofrequencies of Ω_{16^+}, Ω_{19^+}, and Ω_{32^+} are indicated with dashed lines. The main peak occurs at ~Ω_{32^+} gyrofrequency, for both compressional and transverse powers.

$mv^2_{\rm ring}$ and $T_{\parallel} \sim 0$. Therefore, we can estimate the temperature anisotropy caused by the ring distribution by evaluating an effective perpendicular temperature for the ring using the injection velocity of the pickup ions. In this way $T_{\perp j} = m_j v^2_{\perp}/2\kappa_B$, where j refers to the ion species, in this case H_3O^+. If $v_{\perp}$ = 37 km s^{-1} then $T_{\perp H_3O^+} \simeq 0.1356$ keV (consistent with the speed values of *Leisner et al.* [2006]). Parallel temperature is considered very small ($T_{\parallel} < 0.5$ eV, see Table 3). The background plasma consists of H_3O^+, OH^+, O^+, and O_2^+ ions, whose densities correspond to 70%, 15%, and 4% of the total as estimated by the model of *Jurac and Richardson* [2005] for the first three species, respectively. The density of O_2^+ (~1% of the total background density) was estimated from *Martens et al.* [2008].

[19] Figure 8 shows plasma data obtained with CAPS for 2 days of observations: 27 November 2005 and 24 December 2005. The parameters include magnetic field magnitude, density, temperature, and temperature anisotropy for the background H^+ and OH^+ as a function of time and distance. Colored bands identify regions where we have observed ICW and ICW+HMW. The dot-dashed vertical line indicates the closest approach between Cassini and Saturn. We observe that the ICW+HMW intervals occur around the closest approach between Cassini and Saturn, where $\mathbf{B}_{\circ}$ is maximum. We use a total value of $n_{W^+} \simeq 60$ cm^{-3} for the water-group ions resembling CAPS data (see Figure 8) for the region with IC+HM waves and the electron density reported in *Persoon et al.* [2006] and *Tokar et al.* [2008]. The H_3O^+ ring has a density of 8% the total background density, which is consistent with the value estimated by *Tokar et al.* [2008] for the pickup ions. We include a component of electrons to maintain the neutrality in the plasma. The ambient magnetic field is $\mathbf{B}_{\circ}$ = 180 nT, consistent with the value of the magnetic field at the region of ICW+HMW (see Figure 8). The temperature for all species was obtained assuming a total plasma beta of β = 0.0040 ± 0.0008 from *Sittler et al.* [2005] at the Enceladus position, except for the case of OH^+ whose value was obtained from CAPS data (see Figure 8). Figure 8 shows that the background components of the plasma can have a temperature anisotropy with $T_{\perp}/T_{\parallel} \neq 1$, and this can differ for each species. What this is telling us is that the background populations sometimes are not fully thermalized. This is in agreement with previous findings by *Tokar et al.* [2008] where anisotropic plasmas were reported between 4 and 4.5 R_S. With all these values we performed several runs of WHAMP to determine wave growth for ion-cyclotron waves and their harmonic mode (n = 2).

[20] Figure 9 shows wave frequency and growth rate as a function of $\kappa c/\omega_p$ for waves propagating at the fundamental frequency, with $\theta_{B_{\circ\kappa}} \sim 0°$, and waves propagating at the first harmonic frequency (n = 2), with $\theta_{B_{\circ\kappa}} \sim 50°$. We plot dispersion properties for several values of temperature anisotropy ($A = T_{\perp}/T_{\parallel}$) A = 950, A = 2000, and A = 3000. We find that oblique ($\theta_{B_{\circ\kappa}} = 50°$) propagating waves with a frequency of ~2 × Ω_{19^+} corresponding to the first harmonic mode can grow and that their growth rate is much smaller (3–8 times lower at the maximum of growth) than the growth of parallel propagating waves at the fundamental gyrofrequency. This explains why harmonic waves are not observed in all Cassini orbits and why when observed their amplitude is much smaller than waves with a frequency ~Ω_{19^+}. Clearly this figure shows that if the anisotropy $A = \frac{T_{\perp}}{T_{\parallel}}$ increases then the growth of harmonics modes at $\theta_{B_{\circ\kappa}} = 50°$ is enhanced. The growth of harmonic modes requires a large value of temperature anisotropy A which is provided by the pickup ring distributions. We find that for a value of $A > 950$ (corresponding to a bi-Maxwellian with $T_{\perp}$ = 135.6 eV and $T_{\parallel}$ = 0.143 eV) the harmonic mode can grow. In the same way, we find that for a value of $n_{\rm ring} > 2.5$ cm^{-3} the harmonic mode can grow (see Figure 10). Our findings are consistent with the simulation work of *Cowee et al.* [2009], who showed that weak harmonic mode waves with oblique propagation can exist in the Saturnian environment.

[21] Figure 10 presents the behavior of the harmonic mode (n = 2) waves as a function of propagation angle, anisotropy, ring density, and pickup speed. It is clear that these harmonics can grow more at oblique angles (>25° with a maximum growth rate at $\theta_{B_{\circ\kappa}} = 60°$). Figure 10b and Figure 10c show how the grow of the fundamental and their harmonic is enhanced with temperature anisotropy and ring density, respectively. The growth of the fundamental in these cases is always around 2.5–3.5 times the growth of the harmonic mode. From these two plots we can see that the HMW can grow only when temperature anisotropy is $A > 950$. As shown in Figure 10c, harmonic mode waves also require that the ring density $n_{\rm ring} > 2.5$ cm^{-3} (~4.6% of the total background density) for a fixed value of A (A = 1200, corresponding to $T_{\perp}$ = 135.6 eV and $T_{\parallel}$ = 0.113 eV). Below this ring density or anisotropy only waves at the fundamental can grow. The corotation speed of the plasma in Saturn's magnetosphere changes with distance to the planet. For the regions where ICW and HMW are observed during the four orbits analyzed here, the speed varies from 33 km s^{-1} to 53 km s^{-1}, corresponding to distances of 3.5 R_S and 5.5 R_S, respectively [*Russell et al.*, 2006]. Figure 10d shows wave growth for the ion-cyclotron waves at the fundamental, and at $f \sim 2 \times \Omega_{W^+}$, for the extreme pickup ring speeds of 26 and 37 km s^{-1} with

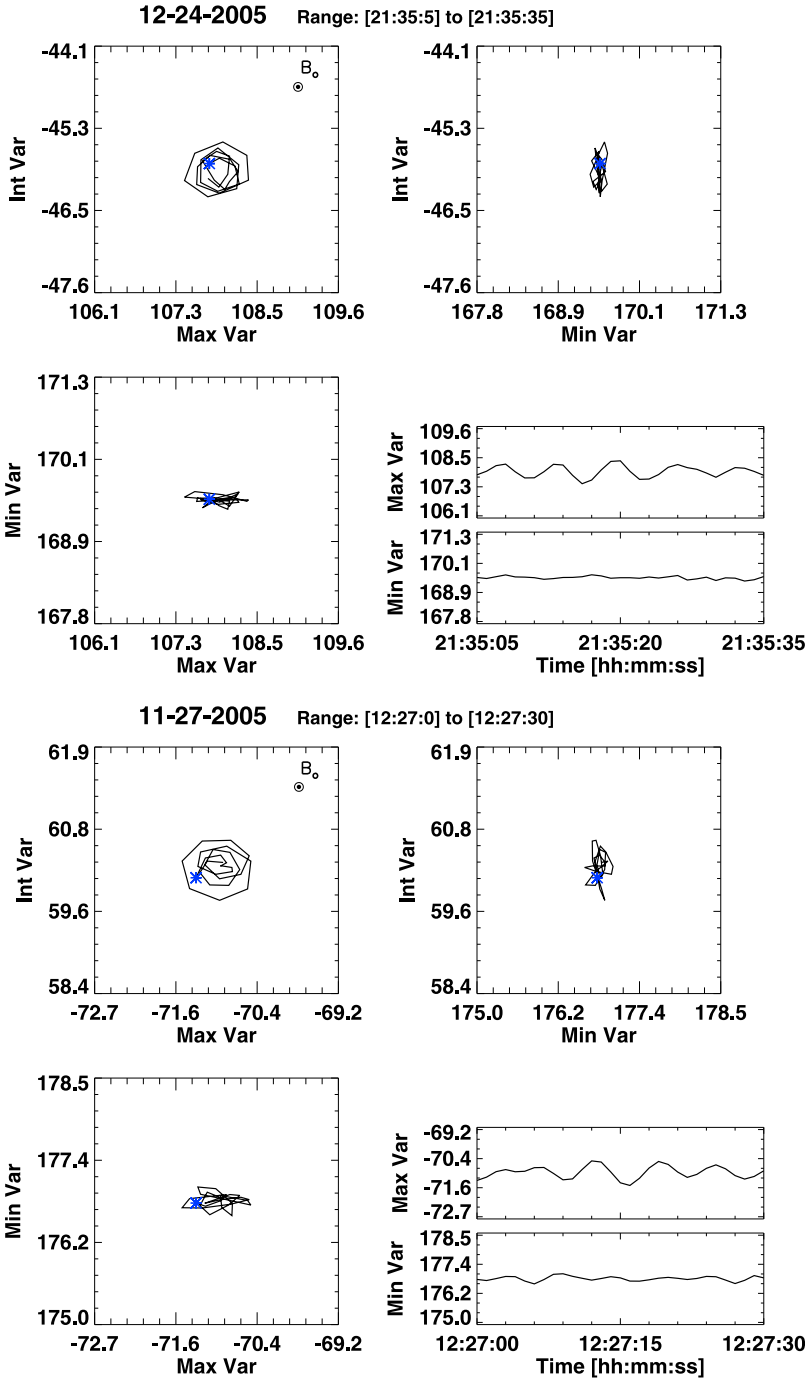

Figure 6. Hodograms for ion-cyclotron waves plus their first harmonic mode for 2 days: 24 December 2005 on the range of [21:35:05–21:35:35] h and 27 November 27th on [12:27:00–12:27:30] h. This analysis shows left-handed polarized waves propagating at oblique angles, $\theta_{Bo\kappa}$, of 34.7° and 27.8° for top and bottom plots, respectively, of the second and fourth representations on the right, with a significant compressive part. The asterisk indicates the beginning of the interval.

a temperature anisotropy A = 1200. We find that wave growth at the fundamental and for the harmonic mode occurs for these two pickup velocities consistent with Cassini observations. If the pickup velocity is much smaller than 26 km s^{-1} the growth of the harmonic mode stops and the waves are damped ($\gamma < 0$), so we do not expect the growth of harmonic mode waves for distances $r \leq 3R_S$. The growth rate is a function of ring velocity with the growth rate increasing for larger $v_\perp$.

4. Discussion and Conclusions

[22] Giant magnetospheres are excellent laboratories to study mass-loading processes and their by-products such as the generation of ion-cyclotron waves. Pioneer 11 made the

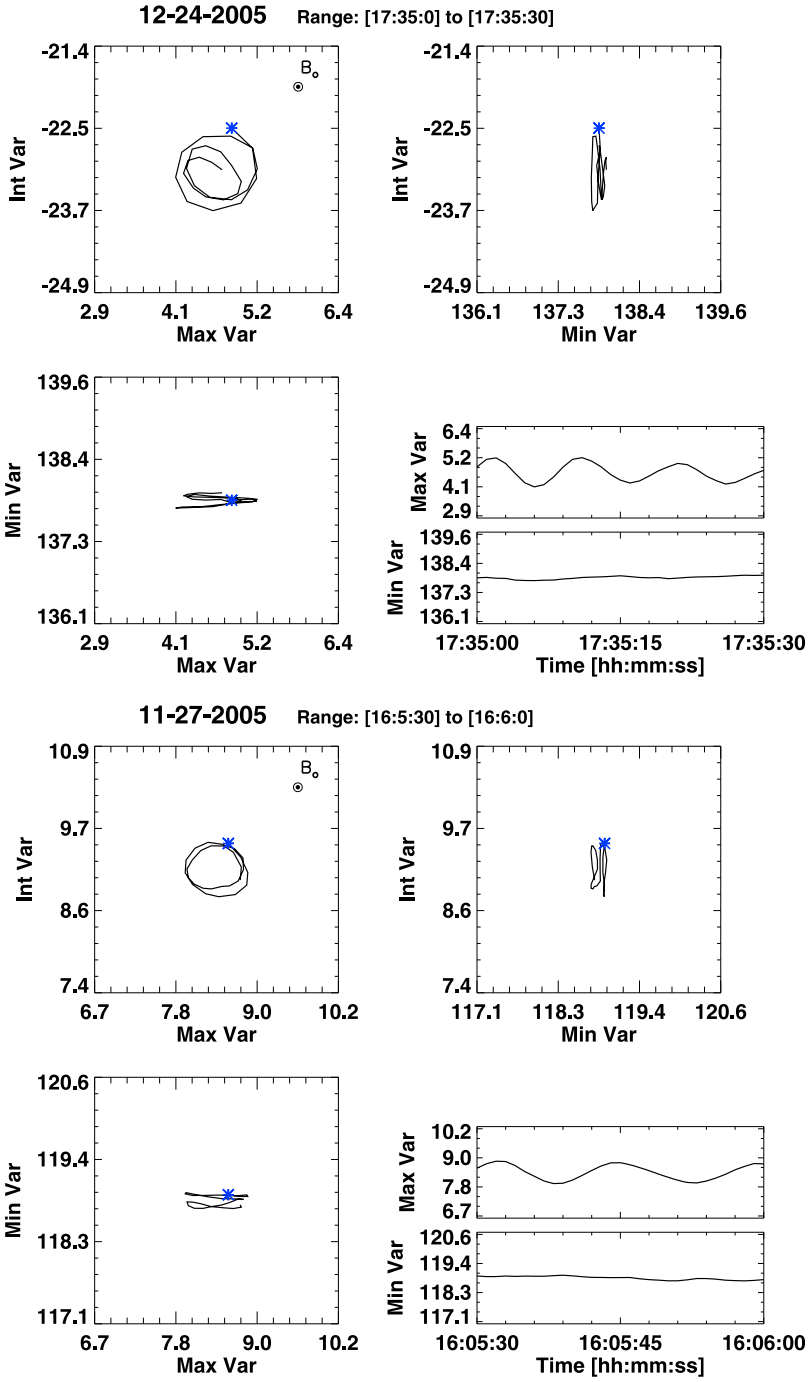

Figure 7. Hodograms for regions where there are just ICW at the fundamental for 2 days: 24 December 2005 on [17:35:00–17:35:30] h and 27 November 2005 on [16:05:30–16:06:00] h. Waves are left handed, propagating almost parallel to the field with $\theta_{Bo\kappa}$ equal to 10° and 6° for the top and bottom plots, respectively, of the second and fourth representations on the right. The asterisk indicates the beginning of the interval.

first detection of ion-cyclotron waves in Saturn's E ring [*Smith and Tsurutani*, 1983]. More recently, Cassini observations revealed that ion-cyclotron waves are commonly observed in Saturn's middle magnetosphere [*Russell et al.*, 2006; *Leisner et al.*, 2006]. These waves have frequencies near the gyrofrequency of water-group ions (O^+, OH^+, H_2O^+, and H_3O^+) and grow via cyclotron resonance from the free energy provided by ions picked up from the E-ring torus. Due to Saturn's field geometry and plasma corotation direction, pickup ions form rings in velocity space with $v_\perp = v_{\rm corot} - V_{\rm Enc}$ and $v_\parallel = 0$ (where $V_{\rm Enc}$ is the Enceladus velocity and $v_{\rm corot}$ is the corotation velocity), so a large temperature anisotropy ($T_\perp > T_\parallel$) arises in the plasma. Waves with longer periods and frequencies matching the gyrofrequency of O_2^+ have also been observed. In most regions these waves have smaller amplitudes than waves generated by water-group

Table 2. MVA Results for Intervals With ICW + HMW and for Intervals Where Only ICW at the Fundamental Were Found

	(ICW + HMW) Region				ICW Region			
Date	Time Interval[a]	$\theta_{B_{o\kappa}}$[b] (°)	$\lambda_{int}/\lambda_{min}$[c]	$\lambda_{max}/\lambda_{int}$[d]	Time Interval	$\theta_{B_{o\kappa}}$ (°)	$\lambda_{int}/\lambda_{min}$	$\lambda_{max}/\lambda_{int}$
09-Mar-05	07:47:45 to 07:48:15	17.1	2.5	1.5	06:40:30 to 06:41:00	13.3	7.3	1.2
17-Feb-05	03:53:23 to 03:53:53	59.0	1.6	1.3	05:52:30 to 05:53:00	11.3	5.6	1.2
24-Dec-05	21:35:05 to 21:35:35	34.7	8.8	1.2	17:35:00 to 17:35:30	9.7	45.7	1.2
27-Nov-05	12:27:00 to 12:27:30	27.8	4.4	1.5	16:05:30 to 16:06:00	6.0	39.8	1.4

[a]Time intervals of MVA.
[b]Angle between the propagation wave vector κ and the unperturbed magnetic field $\mathbf{B}_o$.
[c]Rate between the intermediate and minimum eigenvalues (λ_{int} and λ_{min}).
[d]Rate between the maximum and intermediate eigenvalues (λ_{max} and λ_{int}).

ions but as we mentioned earlier, there are also intervals where waves generated by O_2^+ ions can be dominant.

[23] In this work we have shown the existence of waves with frequencies at twice the gyro–frequency of water-group ions during four orbits of Cassini spacecraft. We have interpreted these waves as a harmonic mode with $n = 2$, and dispersion analysis using WHAMP where ion rings are modeled as highly anisotropic bi-Maxwellians has shown that growth of such waves is possible in a plasma resembling Saturns middle magnetosphere. HM waves occur in regions where also ion-cyclotron waves at the fundamental gyrofrequency are observed. All waves are left hand polarized but the harmonic mode waves propagates at oblique angles (up to 60°) to the ambient field and have a compressive character. While ICW are more parallel propagating and transverse fluctuations. The harmonic mode waves amplitudes are smaller than the ICW, with a power spectrum 2 orders of magnitude less than the power of waves at the fundamental. *Leisner et al.* [2006] found that amplitudes of ICW are variable (0.2–2.0 nT) in time and in space. We have found that the IC+HM waves can have variations in their amplitudes between 0.2 and 0.7 nT.

[24] The variability observed on wave properties imply temporal and spatial changes in the material of the torus. The composition of the pickup ion rings and background plasma is changing, leading to different conditions that affect instability thresholds and the dominant observed mode. The changes of composition of the torus may be related to changes in the chemistry of the material injected to the ring and changes in Enceladus plume and atmosphere.

[25] Using the WHAMP dispersion solver [*Rönmark*, 1982] we have shown that harmonic mode waves can grow in a plasma with the characteristics of Saturn's middle magnetosphere. What is more, linear theory predictions match the characteristics of the HM waves growing in the range of observed $\theta_{B_{o\kappa}}$ angles between 20° and 60°, with maximum growth at ~60°. While ICW have maximum growth at parallel propagation. In agreement with our findings, the growth of harmonic mode waves at Saturn magnetosphere has been suggested by the simulation work of *Cowee et al.* [2009]. Oblique propagating harmonic waves, with maximum growth occurring at $\theta_{B_{o\kappa}} \sim 30°$ have also been found in cometary environments [*Brinca and Tsurutani*, 1989b]. Linear theory has been employed in the past to show that harmonic mode waves can growth in Earth's foreshock with angles of propagation, $\theta_{B_{o\kappa}} \sim 45°$ [*Smith and Gary*, 1987].

[26] Our findings of harmonic mode waves in Saturn's magnetosphere are in contrast to Io where no harmonic modes have been reported from the data even when their growth has been predicted from simulation work [*Cowee et al.*, 2007]. It is probable that HMW are also present near Io but with smaller amplitudes than the waves observed near the SO_2^+, SO^+, and S^+ gyrofrequencies. Unfortunately, the number of Galileo orbits near this moon is limited, so it is also possible that the spacecraft did not sample the regions where harmonic mode growth may be occurring. The region of the E ring extends from 3 R_S to 8 R_S (1 R_S = 60,268 km) from Saturn, so the source region where water-group ions can be picked up to generate waves is much more extended than for Io. Previous works show that ICW are not seen inside 3.8 R_S (from Saturn) and that their amplitudes peak near 4−5 R_S [*Russell and Blanco-Cano*, 2007], i.e., near Enceladus's orbit which is 3.95 R_S from the planet. The study of a large number of orbits shows that the wave-source region is located at the equator, throughout the inner magnetosphere when Cassini is near the equatorial plane [*Leisner et al.*, 2006], with ICW observed within ±0.20 R_S (J. S. Leisner, personal communication, 2009). For the four orbits analyzed here, where we have found that harmonic mode waves tend to be more concentrated at the equator occurring within ±0.04 R_S of the equatorial plane and at distances between 3.8 R_S and 5.5 R_S from Saturn. However, more analysis is required of orbits with high and low inclination angle in order to determine the source region of these ICW and their first harmonic.

Table 3. Plasma Conditions for Dispersion Analysis Used in WHAMP, $|B_o|$ = 180 nT

Specie	Density (cm^{-3})	Temperature, [$T_{\|}$] (eV)	$A = \frac{T_\perp}{T_\|}$	Ring Velocity (km s^{-1})
		Ring		
H_3O^+	4.32	0.02–0.5	6000–250	37
		Background		
H_3O^+	42.00	7.7	4.0	0
OH^+	9.00	40.0	1.0	0
O^+	2.40	134.1	1.0	0
O_2^+	0.60	107.3	1.0	0
Electrons	58.32	6.9	1.0	0

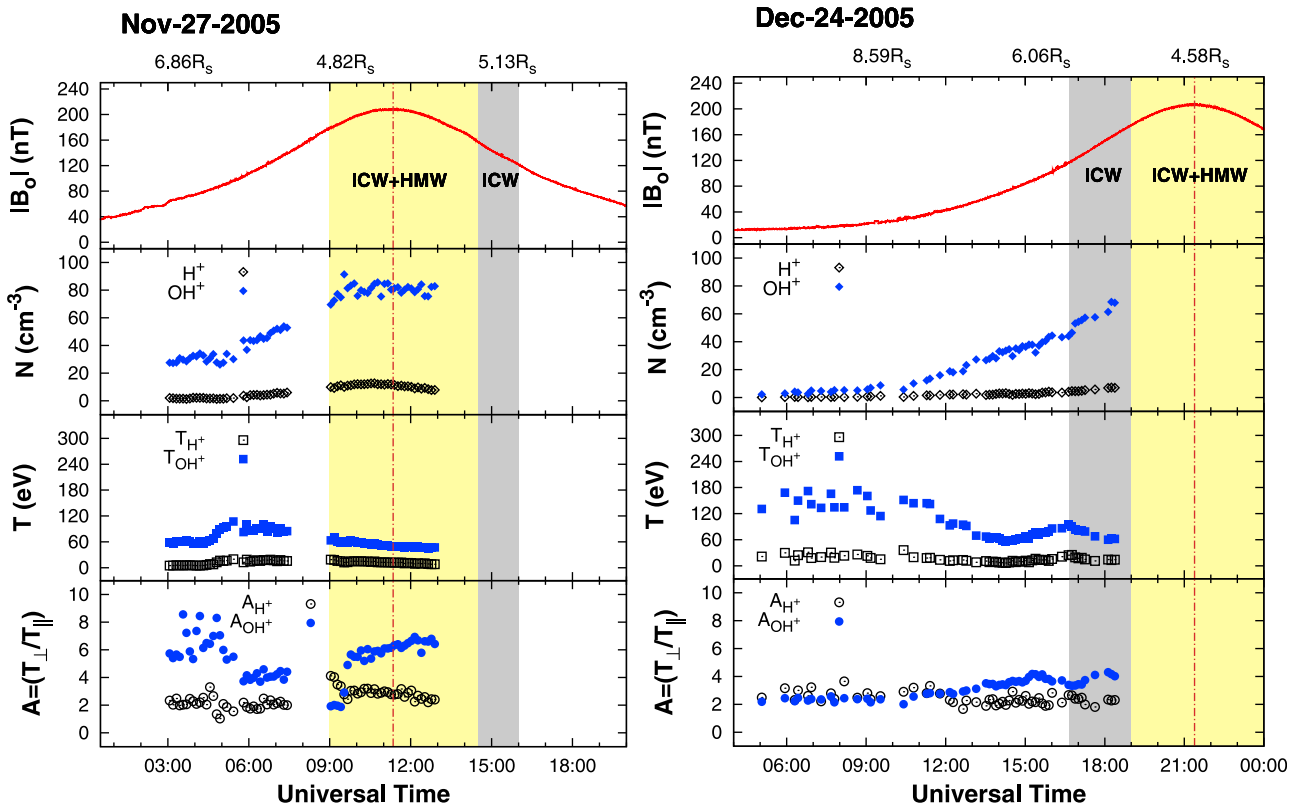

Figure 8. CAPS data for 27 November 2005 and 24 December 2005. From top to bottom the parameters are magnetic field magnitude, density, temperature, and temperature anisotropy for the background H^+ and OH^+ ions. The colored bands identify regions with ICW and ICW+HMW. The dot-dashed vertical line indicates the closest approach between Cassini and Saturn. Distance on the scale above is measured from Saturn's center.

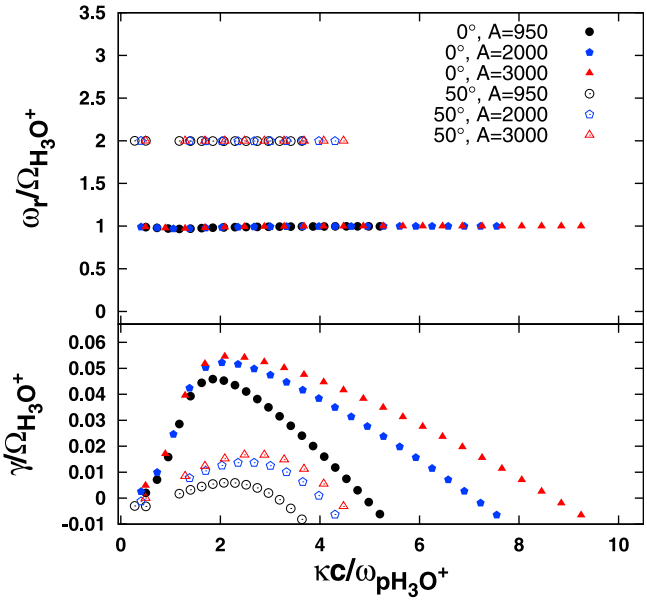

Figure 9. Frequency and growth rate as a function of κ for ion-cyclotron waves and their harmonic mode (n = 2) in a plasma resembling the E-ring environment for several values of anisotropy A. The fundamental mode propagates at $\theta_{B_{o\kappa}}$ = 0° and for the harmonic mode $\theta_{o\kappa}$ = 50°, $\omega_{pH_3O^+}$ is the ion plasma frequency of H_3O^+ ions in the ring with $\omega_{pH_3O^+}$ = 629 Hz, assuming a density of $n_{H_3O^+} = 4.32$ cm^{-3}.

[27] Ion-cyclotron waves and mirror mode grow from temperature (pressure anisotropy) ($T_\perp/T_\parallel > 1$). The dominant mode depends on several factors, such as plasma beta, temperature anisotropy value, and plasma background composition [*Leisner et al.*, 2006]. Studying in detail the properties of waves in the plasma will allow us to enhance our understanding about the changes and processes that the E-ring region suffers. A detailed analysis of mirror mode regions for these four Cassini observations will be presented in a future work.

[28] From WHAMP calculations we have determined the conditions needed in an environment such as Saturn's middle magnetosphere for ICW growth at both the fundamental gyrofrequency and at $f = 2 \times \Omega_{W^+}$. To mimic the growth due to a ring of H_3O^+ ions, we have considered a highly anisotropic bi-Maxwellian and found that there is a critical temperature anisotropy and a ring density value so that the growth of HMW occurs, these values are $A > 950$ (corresponding to $T_\perp$ = 135.6 eV and $T_\parallel$ = 0.143 eV) and $n_{ring} > 2.5$ cm^{-3}, respectively. Below this ring density or anisotropy values only ICW can grow. In fact, ICW can grow for values as low as $n_{ring} \geq 0.5$ cm^{-3} or if $A \geq 250$. Although the use of a dispersion solver code able to model cold ring distributions is desirable, *Cowee et al.* [2007] have shown that WHAMP results when using a highly anisotropic bi-Maxwellian are consistent with the results of modeling a cold ring, so we believe that our predictions represent a good starting point to show that harmonic wave growth is possible at the extended neutral cloud. The interaction of the waves with existing pickup ions may result in ion distribution thermalization and eventually waves may damp. More work is needed to understand the shape of the region permeated with ion-cyclotron waves and harmonic mode waves in Saturn's middle magnetosphere.

[29] Finally, the observable waves amplitudes and characteristics not only are a function of the growth rates of the linear instabilities but also depend on the time that a given wave train spends in the presence of a beam and the mechanism by which the wave saturates and on spcecraft position with respect to the wave source. What is more, waves can be produced by ion rings with different characteristics (cold beams, warm beams which have suffered some thermalization, different beam density, and composition) so in reality the observed spectra are more complex than what linear theory describes. Waves amplitudes can provide a diagnostic of the conditions in the neutral torus. Hybrid simulations can be very useful to study the evolution of fluctuations in mass-loading regions in planetary magnetospheres. They have shown also that there is a linear relation between ion production rate and quasi-steady wave energy level (δB^2) [*Cowee et al.*, 2009].

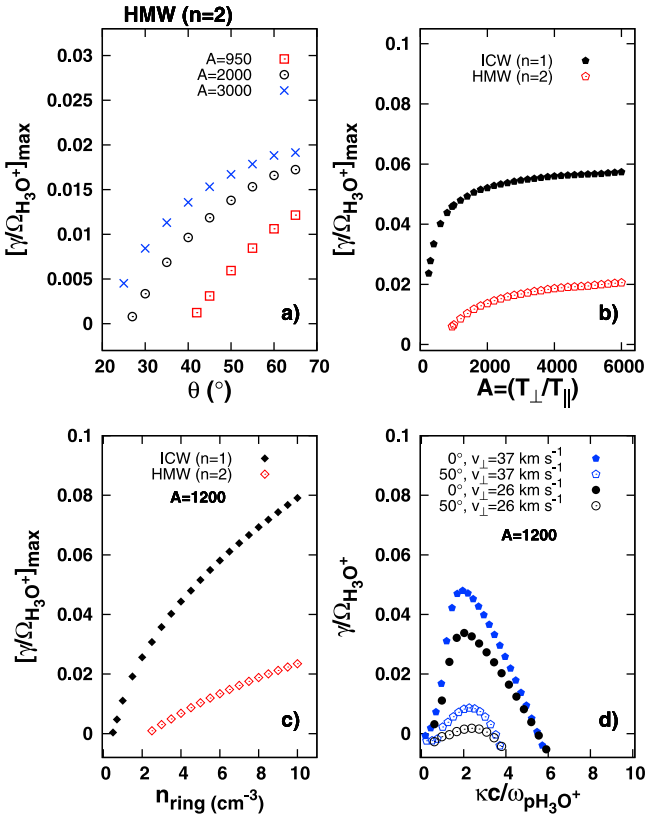

Figure 10. The maximum growth rate for both, ICW and their HMW (n = 2). (a) The growth of HMW as a function of angle of propagation for different anisotropies. (b and c) The growth of HMW as a function of temperature anisotropy and ring density, respectively. From Figures 10b and 10c it is clear that growth of HMW occurs only when $A >$ 950 and if $n_{ring} > 2.5$ cm^{-3} with an anisotropy fixed to the value of A = 1200. (d) The growth of ICW and their first HM for pickup velocity on the range of 37 km s^{-1} and 26 km s^{-1}. When $v_{pickup} < 26$ km s^{-1} the growth of HM cannot occur.

[30] Future work involves the study of large inclination Cassini orbits to determine if HMW can occur out of the equatorial region.

[31] **Acknowledgments.** The authors thank the Cassini–Huygens team and JPL/NASA for the data. Mario Rodríguez-Martínez and Xóchitl Blanco–Cano thank CONACyT, Grant No. 81159. We are grateful to K. Rönmark for the use of the WHAMP solver and thank G. Casillas for the use of the ADO program.

[32] Philippa Browning thanks Andrew Coates and Edward Smith for their assistance in evaluating this paper.

References

Blanco-Cano, X. (2004), Wave generation in moon-satellite interactions, *Adv. Space Res.*, *33*, 2078–2091.

Blanco-Cano, X., C. T. Russell, and R. J. Strangeway (2001a), The Io mass-loading disk: Wave dispersion analysis, *J. Geophys. Res.*, *106*(A11), 26,261–26,276.

Blanco-Cano, X., C. T. Russell, R. J. Strangeway, M. G. Kivelson, and K. K. Khurana (2001b), Galileo observations of ion cyclotron waves in the Io torus, *Adv. Space Res.*, *28*, 1469–1474.

Brinca, A. L. (1991), *Cometary Linear Instabilities: From Profusion to Perspective, Geophys. Monogr. Ser.*, vol. 61, pp. 211–221, AGU, Washington, D. C.

Brinca, A. L., and B. T. Tsurutani (1989a), On the excitation of cyclotron harmonic waves by newborn heavy ions, *J. Geophys. Res.*, *94*(A5), 5467–5473.

Brinca, A. L., and B. T. Tsurutani (1989b), The oblique behavior of low-frequency electromagnetic waves excited by newborn cometary ions, *J. Geophys. Res.*, *94*(A1), 3–14.

Cowee, M. M., C. T. Russell, R. J. Strangeway, and X. Blanco-Cano (2007), One-dimensional hybrid simulations of obliquely propagating ion cyclotron waves: Application to ion pickup at Io, *J. Geophys. Res.*, *112*, A06230, doi:10.1029/2006JA012230.

Cowee, M. M., N. Omidi, C. T. Russell, X. Blanco-Cano, and R. L. Tokar (2009), Determining ion production rates near Saturn's extended neutral cloud from ion cyclotron wave amplitudes, *J. Geophys. Res.*, *114*, A04219, doi:10.1029/2008JA013664

Dougherty, M. K., et al. (2004), The Cassini magnetic field investigation, *Space Sci. Rev.*, *114*, 331–383.

Dougherty, M. K., K. K. Khurana, F. M. Neubauer, C. T. Russell, J. Saur, J. S. Leisner, and M. E. Burton (2006), Identification of a dynamic atmosphere at Enceladus with the Cassini magnetometer, *Science*, *311*, 1406–1409.

Fleshman, B. L., P. A. Delamere, and F. Bagenal (2010), Modeling the Enceladus plume–plasma interaction, *Geophys. Res. Lett.*, *37*, L03202, doi:10.1029/2009GL041613.

Gary, S. P. (September 1993), *Theory of Space Plasma Microinstabilities*, edited by S. Peter Gary, p. 193, Cambridge, UK, Cambridge University Press.

Glassmeier, K.-H., A. J. Coates, M. H. Acuna, M. L. Goldstein, A. D. Johnstone, F. M. Neubauer, and H. Reme (1989), Spectral characteristics of low-frequency plasma turbulence upstream of Comet P/Halley, *J. Geophys. Res.*, *94*(A1), 37–48.

Hansen, C. J., L. Esposito, A. I. F. Stewart, J. Colwell, A. Hendrix, W. Pryor, D. Shemansky, and R. West (2006), Enceladus' water vapor plume, *Science*, *311*, 1422–1425.

Hoppe, M. M., C. T. Russell, L. A. Frank, T. E. Eastman, E. W. Greenstadt (1981), Upstream hydromagnetic waves and their association with backstreaming ion populations: ISEE 1 and 2 observations, *J. Geophys. Res.*, *86*(A6), 4471–4492.

Huddleston, D. E., and A. D. Johnstone (1992), Relationship between wave energy and free energy from pickup ions in the Comet Halley environment, *J. Geophys. Res.*, *97*(A8), 12,217–12,229.

Huddleston, D. E., R. J. Strangeway, X. Blanco-Cano, C. T. Russell, M. G. Kivelson, and K. K. Khurana (1999), Mirror-mode structures at the Galileo-Io flyby: Instability criterion and dispersion analysis, *J. Geophys. Res.*, *104*(A8), 17,479–17,490.

Johnson, R. E., et al. (2006), Production, ionization and redistribution of O_2 in Saturn's ring atmosphere, *Icarus*, *180*, 393–402.

Jurac, S., and J. D. Richardson (2005), A self-consistent model of plasma and neutrals at Saturn: Neutral cloud morphology, *J. Geophys. Res.*, *110*, A09220, doi:10.1029/2004JA010635.

Khurana, K. K., M. K. Dougherty, C. T. Russell, and J. S. Leisner (2007), Mass loading of Saturn's magnetosphere near Enceladus, *J. Geophys. Res.*, *112*, A08203, doi:10.1029/2006JA012110.

Kivelson, M. G. (2006), Does Enceladus govern magnetospheric dynamics at Saturn?, *Science*, *311*, 1391–1392.

Leisner, J. S., C. T. Russell, M. K. Dougherty, X. Blanco-Cano, R. J. Strangeway, and C. Bertucci (2006), Ion cyclotron waves in Saturn's E ring: Initial Cassini observations, *Geophys. Res. Lett.*, *33*, L11101, doi:10.1029/2005GL024875.

Martens, H. R., D. B. Reisenfeld, J. D. Williams, R. E. Johnson, H. T. Smith (2008), Observations of molecular oxygen ions in Saturn's inner magnetosphere, *Geophys. Res. Lett.*, *35*, L20103, doi:10.1029/2008GL035433.

Persoon, A. M., D. A. Gurnett, W. S. Kurth, and J. B. Groene (2006), A simple scale height model of the electron density in Saturn's plasma disk, *Geophys. Res. Lett.*, *33*, L18106, doi:10.1029/2006GL027090.

Rönmark, K. (1982), WHAMP: Waves in Homogeneous, Anisotropic, Multicomponent Plasmas, *Kiruna Geophys. Inst. KGI Report 179*, Univ. of Umea, Kiruna, Sweden.

Russell, C. T., and X. Blanco-Cano (2007), Ion-cyclotron wave generation by planetary ion pickup, *J. Atmos. Sol. Terr. Phys.*, *69*, 1723–1738.

Russell, C. T., J. S. Leisner, C. S. Arridge, M. K. Dougherty, and X. Blanco-Cano (2006), Nature of magnetic fluctuations in Saturn's middle magnetosphere, *J. Geophys. Res.*, *111*, A12205, doi:10.1029/2006JA011921.

Sittler, E. C., et al. (2005), Preliminary results on Saturn's inner plasmasphere as observed by Cassini: Comparison with Voyager, *Geophys. Res. Lett.*, *32*, L14S07, doi:10.1029/2005GL022653.

Smith, C. W., and S. P. Gary (1987), Electromagnetic ion beam instabilities: Growth at cyclotron harmonic wave numbers, *J. Geophys. Res.*, *92*(A1), 117–125.

Smith, C. W., M. L. Goldstein, and W. H. Matthaeus (1983), Turbulence analysis of the Jovian upstream 'wave' phenomenon, *J. Geophys. Res.*, *88*(A7), 5581–5593.

Smith, E. J., and B. T. Tsurutani (1983), Saturn's magnetosphere: Observations of ion cyclotron waves near the Dione L shell, *J. Geophys. Res.*, *88*(A10), 7831–7836.

Storey, L. R. O., and F. Lefeuvre (1979), The analysis of 6-component measurements of a random electromagnetic wave field in a magnetoplasma. I. The direct problem, *Geophys. J. Int.*, *56*, 255–269.

Tan, L. C., G. M. Mason, and B. T. Tsurutani (1993), Evidence for proton cyclotron waves near Comet Giacobini-Zinner, *Geophys. Res. Lett.*, *20*(3), 169–172.

Tokar, R. L., et al. (2006), The interaction of the atmosphere of Enceladus with Saturn's plasma, *Science*, *311*, 1409.

Tokar, R. L., et al. (2008), Cassini detection of water-group pick-up ions in the Enceladus torus, *Geophys. Res. Lett.*, *35*, L14202, doi:10.1029/2008GL034749.

Tsurutani, B. T. (1991), *Comets: A Laboratory for Plasma Waves and Instabilities*, *Geophys. Monogr. Ser.*, 61, 189–209, AGU, Washington, D. C.

Wilson, R. J., R. L. Tokar, M. G. Henderson, T. W. Hill, M. F. Thomsen, and D. H. Pontius (2008), Cassini plasma spectrometer thermal ion measurements in Saturn's inner magnetosphere, *J. Geophys. Res.*, *113*, A12218, doi:10.1029/2008JA013486.

Wong, H. K., M. L. Goldstein, and C. W. Smith (1991), Ion cyclotron harmonic resonances driven by ion ring-beam distributions, *J. Geophys. Res.*, *96*(A1), 285–288.

Young, D. T., et al. (2004), Cassini plasma spectrometer investigation, *Space Sci. Rev.*, *114*, 1–4.

Young, D. T., et al. (2005), Composition and dynamics of plasma in Saturn's magnetosphere, *Science*, *307*, 1262–1266.

X. Blanco-Cano and M. Rodríguez-Martínez, Instituto de Geofísica, Departamento de Ciencias Espaciales, Universidad Nacional Autónoma de México, Ciudad Universitaria C.P., 04510, México. (mario@geofisica.unam.mx)

M. K. Dougherty, Blackett Laboratory, Department of Physics, Imperial College, London, UK.

J. S. Leisner, Department of Physics and Astronomy, University of Iowa, Iowa City, IA 52242, USA.

C. T. Russell, Institute of Geophysics and Planetary Physics, University of California, 100 Stein Plaza Driveway, Los Angeles, CA 90095-7065, USA.

R. J. Wilson, Laboratory for Atmospheric and Space Physics, University of Colorado at Boulder, Boulder, CO, USA.